Effect of Pressure on the Adsorption Rate for Gasoline Vapor on Pitch-Based Activated Carbon†

J.M. He, K.C. Ng,* C. Yap, and B.B. Saha

Department of Mechanical Engineering, National University of Singapore, 10 Kent Ridge Crescent, Singapore 119260

In this paper, the adsorption kinetics of gasoline vapor on pitch-based activated carbon is experimentally investigated. The main objective is to explore the effect of initial bed pressure on the adsorption rate. The experiments have been conducted by using a thermogravimetric analyzer (TGA) unit, which has a precision of ± 0.1 μg in measuring the adsorption uptake, at adsorption temperatures of 30 °C and 35 °C which are useful for gasoline emission control. Pressure is found to influence the adsorption rate and uptake. The adsorption rate constants or effective mass transfer coefficients are correlated with the pressure differences between the gasoline vapor and the adsorption chamber. This study suggests that the effect of the initial pressure of the adsorption chamber should be taken into account in calculating the adsorption kinetics for the simulation of a practical adsorption process.

Introduction

Environmental pollution caused by gasoline vapor emitted during vehicle operation and idling, gasoline distribution, and refueling at gas stations has drawn much attention[1,2] because the gasoline vapor leads to the destruction of ozone and aids in the production of photochemical smog. Adsorption of gasoline vapor using activated carbon is one of the effective methods for gasoline evaporative emission control and vapor recovery. For the modeling of this adsorption process, the adsorption characteristics over broad operating conditions are needed. The adequacy and reliability of modeling such adsorption processes depend on the accuracy of fundamental parameters such as the adsorption isotherm and kinetics. Adsorption kinetics is of critical importance in modeling the adsorption process and assessing the performance of the activated carbon bed. The Linear Driving Force (LDF) approximation[3] is widely accepted because it directly relates the average amount adsorbed in a particle to the overall amount adsorbed, which simplifies the mathematical modeling. A number of research studies[4−9] adapted the LDF model to correlate adsorption kinetic data for the adsorption of hydrocarbon gases onto activated carbon and found that the LDF is valid for most parts of the isotherms. However, the investigation of the adsorption kinetics of gasoline vapor by activated carbon is very limited. El-Sharkawy et al.[10] investigated the isotherm and kinetics of gasoline adsorption on activated carbon of type Maxsorb III and activated carbon fiber of type ACF1500 under partial vacuum conditions (system pressure below 10 kPa). The adsorption isotherms of gasoline vapor onto activated carbon and DAY zeolite have also been studied by Ryu et al.[11,12] using a static volume method (for system pressure up to 8 kPa).

For experimental adsorption characteristic studies, a "clean" or "out-gassed" adsorbent surface is required,[13] and such a condition is usually obtained by vacuum outgassing or a gas displacement process. This implies that the adsorption takes place on initially "zero" loaded adsorbent surfaces. However, in a gasoline adsorption process of the vehicle emission control system, the adsorption usually occurs at near or just below the atmospheric condition. Therefore, the objective of this study is to investigate the adsorption rate and uptake under various initial adsorption chamber pressures rather than that of a partially vacuumed and outgassed chamber. Since the initial adsorption chamber condition is closer to the real application, the experimental findings in this study could be useful for the practical design and modeling of the adsorption processes for gasoline vehicle evaporative emission control.

Experimental Section

The adsorption experiments were conducted based on the gravimetric method by using a thermogravimetric analyzer (TGA) apparatus. Figures 1(a) and 1(b) show a schematic diagram and pictorial view of the TGA apparatus which comprises the TGA units, a temperature-controlled evaporator, a vacuum pump, and a pressure-control modulating valve. The instantaneous adsorption uptake can be measured by a microbalance with a precision of 0.1 μg. The reaction chamber (adsorption) temperature was controlled by a built-in microprocessor and measured by a type K thermocouple which was inserted into the reaction chamber near the bottom of the adsorbent sample bowl. The adsorption chamber pressure was modulated and maintained through a butterfly modulating valve which was controlled by a MKS pressure controller (model 631A) and a MKS Baratron pressure transducer (type 631A) with an uncertainty of ± 0.15 % of the full range (100 kPa). A diaphragm type vacuum pump was used to evacuate the system, incorporating the pressure controller and modulating valve to maintain a preset chamber pressure. Stainless steel porous filters were installed at the inlet and outlet of the reaction chamber to minimize the pressure fluctuation arising from the modulating action. Helium gas was introduced from the top of the reaction chamber to protect the microbalance from any reactive gases and also to obtain the preset chamber pressure. In addition, the temperature and pressure of gasoline vapor inside the evaporator were monitored and measured by a RTD temperature sensor (± 0.1 °C) and a "Kyowa" pressure transducer (PGS-10A, 0.07 % of scale range), respectively.

* Corresponding author. E-mail: mpengkc@nus.edu.sg. Tel.: (65) 65162214. Fax: (65) 67791459.

† Part of the "Gerhard M. Schneider Festschrift".

10.1021/je800809k CCC: $40.75
Published on Web 03/24/2009

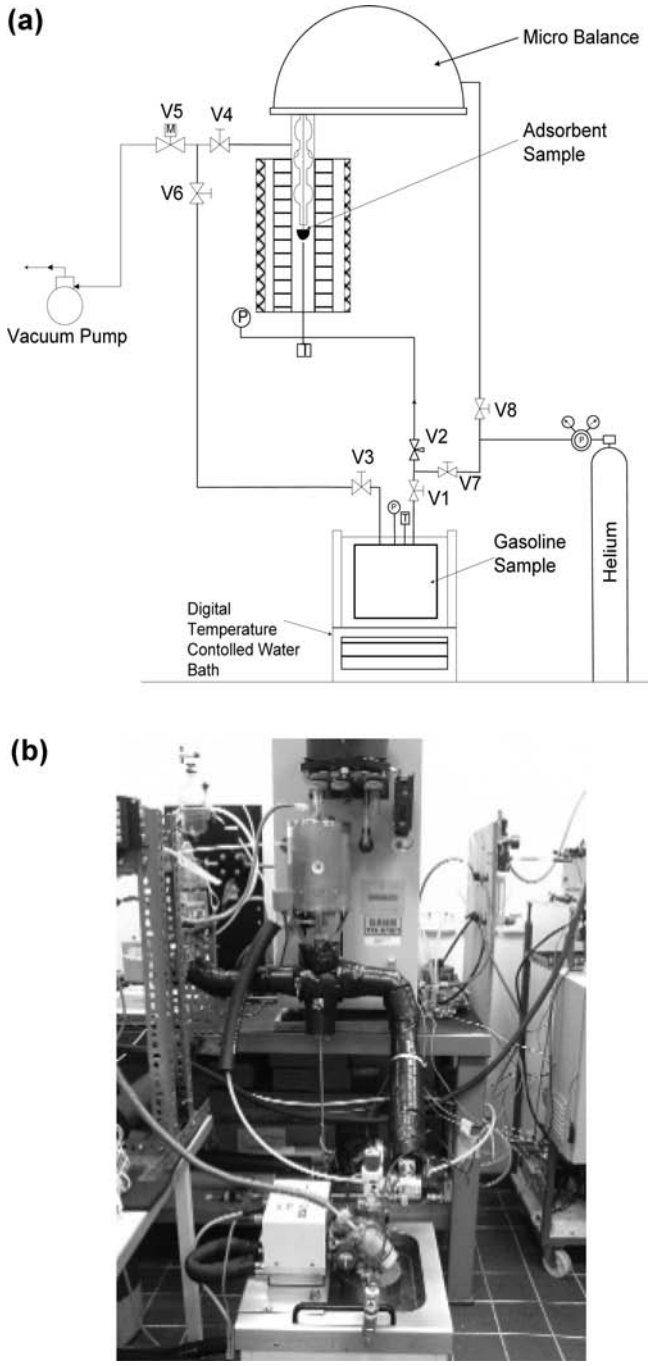

Figure 1. (a) Schematic diagram of the TGA apparatus. (b) Pictorial view of the TGA apparatus.

Activated carbon of type Maxsorb III,[14] developed by the Kansai Coke & Chemicals Co. Ltd., Japan, was used as the adsorbent. It has a high surface area (3010 $m^2 \cdot g^{-1}$), large pore volume (1.7 $mL \cdot g^{-1}$), and small pore diameter (average 7.0 nm). Commercial gasoline (Octane 98) is used throughout the experiment. Typical components of the gasoline are tabulated in Table 1, in terms of volumetric percentage.

The Maxsorb III sample, typically about 87 mg ± 0.1 mg, was first weighed in the moisture analyzer (Computrac Max 5000) before loading it into the TGA. Then it was heated "in situ" at 140 °C for several hours. Finally, it was placed in the sample bowl of the TGA. The dry mass was recorded. Prior to each adsorption test, the sample was first regenerated under vacuum conditions at a temperature of 140 °C and is maintained for several hours to ensure thorough desorption.

Table 1. Composition of Gasoline[a]

component	percentage/% (by volume)
paraffins	40.4
olefins	20.5
napthenes	4.3
aromatics	33.0
benzene	1.8

[a] Tested by SGS Testing & Control Services Singapore Pte, Ltd. in accordance with the Method ASTM-D 6293-98(3).

Prior to each adsorption test, the initial adsorption chamber pressure was obtained by injecting low density helium gas from the top of the TGA into the reaction chamber. This chamber pressure can be set and maintained by the pressure-controlled modulating valve. Meanwhile, a sample mass was continuously monitored before and after introduction of helium for more than an hour to ensure that no adsorption of helium by activated carbon took place. This point is further elaborated later in this paper. Gasoline inside the evaporator was first cooled to 10 °C and evacuated repeatedly to make sure that there was no vapor in the void space of the evaporator. Then the helium was charged into the evaporator through valves V1 and V7 until the pressure reached 65 kPa. This pressure was always maintained for each test. Gasoline was then heated to 30 °C, reaching the pressure of 92 kPa, which was maintained continuously. This initial evaporator pressure was recorded. For each test, full fresh gasoline of the same volume was always refilled to ensure consistent vapor temperature and pressure.

After the reaction chamber temperature and pressure stabilized, the adsorption test was started by opening the valves V1 and V2 between the evaporator and reaction chamber. By regulating the needle valve V2, the gasoline vapor flowed slowly into the reaction chamber through the connecting tube. All parameters including adsorbent sample mass, pressures, and temperatures were recorded at intervals of 5.0 s by the HP data acquisition unit until the equilibrium condition was reached. A set of adsorption experiments were carried out at various initial chamber pressures ranging from 30 kPa to 71 kPa or corresponding pressure difference ($\Delta P = P_e - P_c$, where P_e is the evaporator pressure and P_c is the chamber pressure) from 21 kPa to 62 kPa under adsorption temperatures of 30 °C and 35 °C.

Results and Discussion

Correlation of Experimental Results. To evaluate the adsorption kinetics of gasoline vapor onto activated carbon, the well-known linear driving force (LDF) approximation[3] is used and expressed as

$$\frac{dw}{dt} = k_s a_v \cdot (W - w) \quad (1)$$

where $k_s a_v$ is the adsorption rate constant or LDF effective mass transfer coefficient; w is the instantaneous uptake ($g \cdot g^{-1}$); and W is the corresponding equilibrium adsorption uptake ($g \cdot g^{-1}$). Equation 1 can be rearranged as

$$\frac{dw}{(W - w)} = k_s a_v \cdot dt \quad (2)$$

By integrating both sides of eq 2 with initial condition $t = 0$, $w = 0$, one can get

$$\int_0^w \frac{dw}{W-w} = \int_0^t k_s a_v \cdot dt$$

i.e.

$$-\ln(W-w)|_0^w = k_s a_v \cdot t|_o^t$$

which implies

$$\ln\frac{(W-w)}{W} = -k_s a_v \cdot t \quad (3)$$

Hence, the effective mass transfer coefficient $k_s a_v$ can be determined from the gradient of the plot of $\ln[(W-w)/W]$ versus time. Rearranging eq 3, the predicted uptake is expressed as

$$w = W \cdot (1 - e^{-k_s a_v \cdot t}) \quad (4)$$

To evaluate the effect of pressure, "transition state theory" is introduced in this study. It is assumed that there is a transient thermodynamic equilibrium between the reactants and transition complex, which is expressed by[15]

$$\Delta G = \Delta H - T \cdot \Delta S = -RT \cdot \ln K^* \quad (5)$$

where ΔG is Gibbs energy change for formation of the transition state; ΔH is the enthalpy change in the formation of the transition state; and ΔS is the entropy change of formation of the transition state. K^* is the equilibrium constant for the transition state.

For the isothermal adsorption process, eq 5 is partially differentiated with respect to pressure, giving

$$-\left[\frac{\partial(\Delta G)}{\partial P}\right]_T = -\Delta V = RT \cdot \left[\frac{\partial(\ln K^*)}{\partial P}\right]_T \quad (6)$$

By assuming that the system is incompressible, i.e., ΔV does not vary with pressure, then integrating eq 6 at constant temperature gives

$$\ln K^* = -P\Delta V/RT + C_1 \quad (7)$$

where C_1 is a constant. In transition theory, the rate constant ($k_s a_v$) in eq 1 is proportional to the equilibrium constant K^*, which can be expressed in logarithmic form[15]

$$\ln k_s a_v = \ln K^* + C_2 \quad (8)$$

where C_2 is a constant. Thus, by substituting the value of $\ln K^*$ by eq 7, we can obtain

$$\ln k_s a_v = -P\Delta V/RT + C \quad (9)$$

where C ($= C_1 + C_2$) is a constant. P is the chamber pressure which can be expressed by $P = P_e - \Delta P$. Thus, eq 9 can be further expressed as

$$\ln k_s a_v = -(P_e - \Delta P)\Delta V/RT + C = \Delta P \cdot \Delta V/RT - P_e/RT + C$$

Under constant adsorption temperature, T, and a constant evaporator condition, i.e., P_e is constant, $C' = -P_e/RT + C$ is constant. Therefore

$$\ln k_s a_v = \Delta P \cdot \Delta V/RT + C' \quad (10)$$

Therefore, under isothermal adsorption, a plot of $\ln(k_s a_v)$ versus ΔP should be linear. Moreover, the correlation of the rate constant ($k_s a_v$) with ΔP can be described by rearranging eq 10 in the following form

$$k_s a_v = \exp\left(\frac{\Delta P \cdot \Delta V}{RT}\right) \cdot \exp(C') = \exp\left[\Delta P \cdot \left(\frac{\Delta V}{RT}\right)\right]\exp(C') \quad (11)$$

Under a certain adsorption temperature, T, and assuming an incompressible system, $(\Delta V)/(RT)$ is constant, thus eq 11 can be further simplified t

$$k_s a_v = C_T' \cdot \exp(C_T \cdot \Delta P) \quad (12)$$

where

$$C_T = \frac{V}{RT};\ C_T' = \exp(C')$$

From another point of view, the effective mass transfer coefficient $k_s a_v$ can be expressed as the function of the surface diffusion as given by eq 13[3]

$$k_s a_v = \frac{F_o \cdot D_s}{Rp^2} \quad (13)$$

where F_o is a constant; D_s is the surface diffusion; and R_p is the particle radius. The relation between the surface diffusion and adsorption temperature can be given by the Arrhenius form as expressed by eq 14

$$D_s = D_{so} \cdot \exp\left(\frac{-E_a}{RT}\right) \quad (14)$$

where E_a is the activation energy of the adsorbate. D_{so} is a pre-exponential constant that varies with the pressure differences. To apply eq 14 into eq 13, the effective mass transfer coefficient $k_s a_v$ can be expressed

$$k_s a_v = D_{so}^*(\Delta P) \cdot \exp\left(\frac{-\overline{E_a}}{RT}\right) \quad (15)$$

where $\bar{E}_a$ represents the molar weighted activation energy of gasoline vapor and has been obtained experimentally (39 $kJ \cdot mol^{-1}$)[16] and $D_{so}^*(\Delta P)$ equal to $F_o D_{so}/R_p^2$ is a function of pressure difference ΔP.

Effect of Helium Gas on the Adsorption Measurement. To identify the accuracy of the experiment, the effect of helium gas

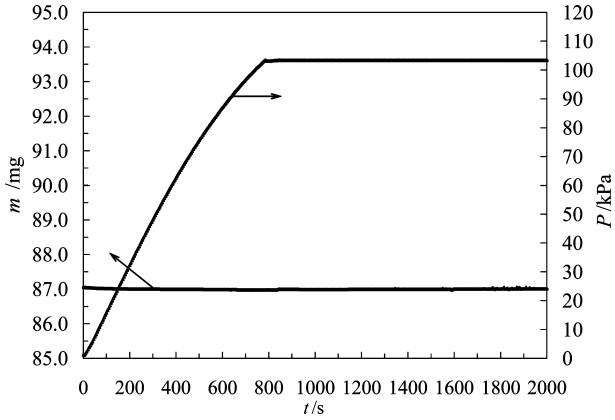

Figure 2. Adsorbent sample mass and adsorption chamber pressure vs time during charging of helium gas.

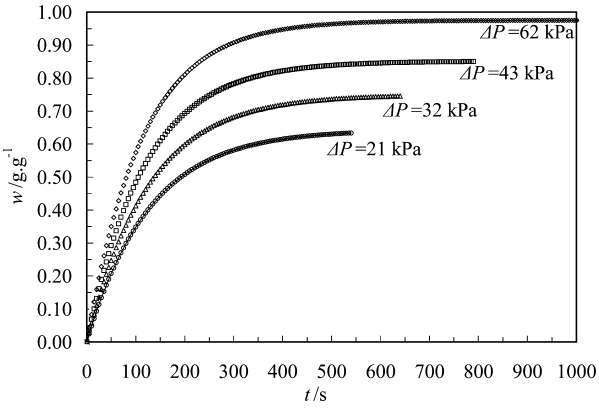

Figure 3. Adsorption uptakes vs time at various pressure differences ΔP under an adsorption temperature of 30 °C.

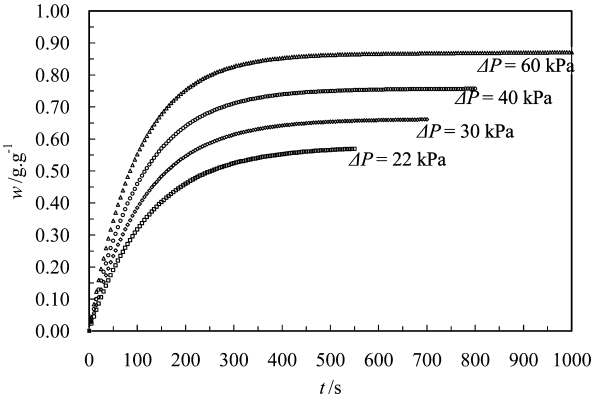

Figure 4. Adsorption uptakes vs time at various pressure differences ΔP under adsorption temperature of 35 °C.

on the adsorption measurement was first investigated. The reaction chamber pressure was continuously increased from 1.6 kPa to 103.3 kPa when charging the helium; meanwhile, the sample mass was recorded as shown in Figure 2. The result shows that the adsorbent mass remains almost stable, and no adsorption of helium occurs within the experimental range. Therefore, it can be confirmed that helium gas does not affect the adsorption uptake measurement in this study.

Adsorption Uptake. Figures 3 and 4 show the transient changes of adsorption uptake versus time under the adsorption temperature of 30 °C and 35 °C, respectively. Experiments have been carried out at various pressure differences ranging from 21 kPa to 62 kPa. It can be seen that the larger the pressure difference, the faster and higher are the adsorption uptakes, for example, 0.55 $g \cdot g^{-1}$ at 62 kPa and 0.38 $g \cdot g^{-1}$ at 21 kPa in the first 60 s at an adsorption

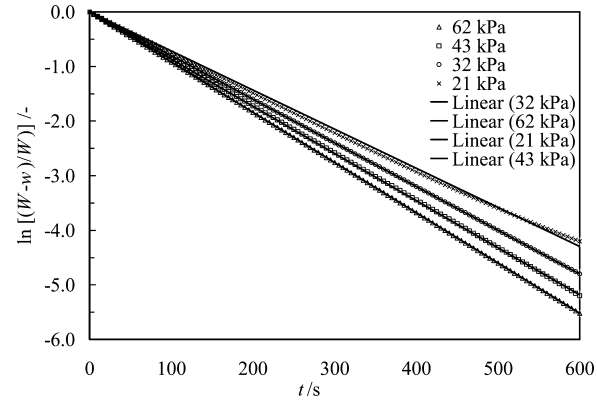

Figure 5. ln[($W - W$)/W] vs time under an adsorption temperature of 30 °C.

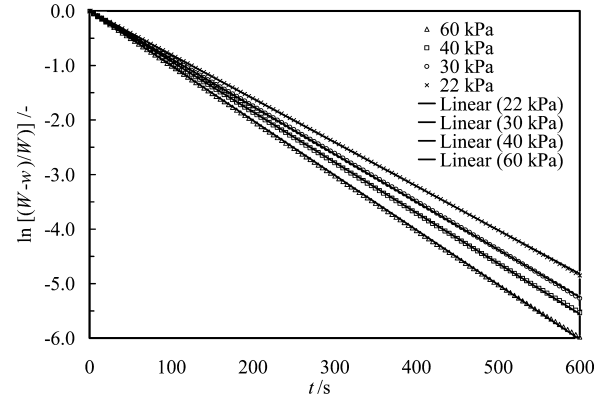

Figure 6. ln[($W - W$)/W] vs time under an adsorption temperature of 35 °C.

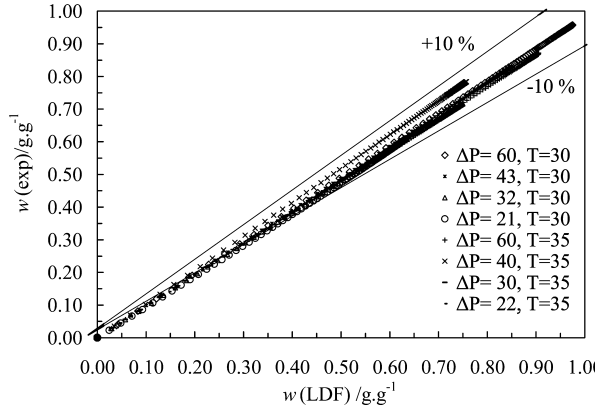

Figure 7. Deviation between LDF predicted uptake w(LDF) and experimental uptake w(exp) at various pressure differences and two adsorption temperatures (ΔP in kPa, T in °C).

temperature of 30 °C. This scenario can be explained that, under high pressure difference or low chamber pressure, the partial pressure of gasoline vapor is higher and the vapor molecules can transport more easily through bulk helium gas and then diffuse within particles to the adsorption sites. In contrast, under low pressure difference or high chamber pressure, the higher partial pressure helium gas retards the gasoline hydrocarbon vapor molecules to reach the pore wall and then to particle adsorption sites. The vapor molecules have to traverse through the spaces occupied by helium gas and then diffuse within the adsorbent particles. The equilibrium uptake is also higher at higher pressure differences of 0.98 $g \cdot g^{-1}$ at 62 kPa compared to 0.65 $g \cdot g^{-1}$ at 21 kPa (at an adsorption temperature of 30 °C), which indicates a 50 % increase in uptake with a three-time increase in pressure

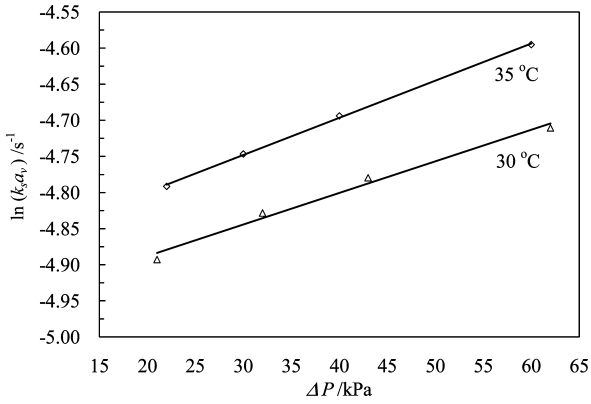

Figure 8. ln(k_sa_v) vs pressure difference under adsorption temperatures of 30 °C and 35 °C.

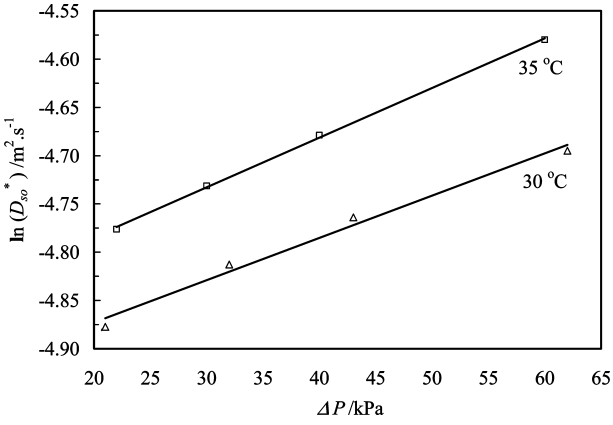

Figure 9. D_{so}* vs pressure difference under adsorption temperatures of 30 °C and 35 °C.

Table 2. Adsorption Rate Constant k_sa_v for Two Different Adsorption Temperatures T and Various Pressure Differences ΔP

adsorption temperature (°C)	ΔP (kPa)	k_sa_v (s^{-1})
$T = 30.0$	21.0	0.00750
	32.0	0.00800
	43.0	0.00840
	62.0	0.00900
$T = 35.0$	22.0	0.00833
	30.0	0.00868
	40.0	0.00914
	60.0	0.01013

difference. It can be concluded that, under lower initial bed pressure, the higher adsorption rate and uptake can be expected. Therefore, a lower initial bed pressure is very useful for a higher adsorption rate and uptake, which can be achieved by a form of vacuuming, but it is also constrained by the system conditions.

Pressure Effect on the Adsorption Rate Constant. The plots of ln[$(W - w)/W$] versus time under various pressure differences at adsorption temperatures of 30 °C and 35 °C are shown in

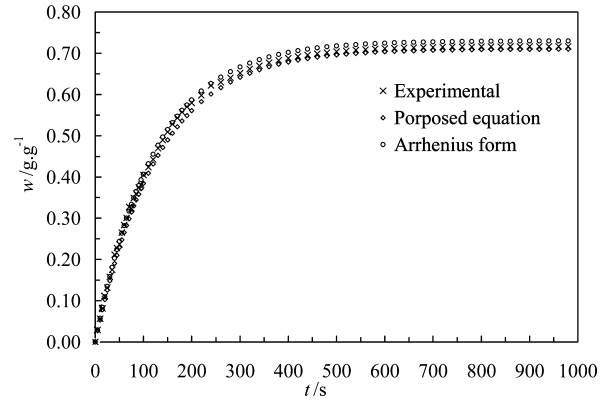

Figure 10. Comparison of experimental adsorption uptake w, predicted uptake w, and uptake w determined by the Arrhenius form at pressure differences of 32 kPa under an adsorption temperature of 30 °C.

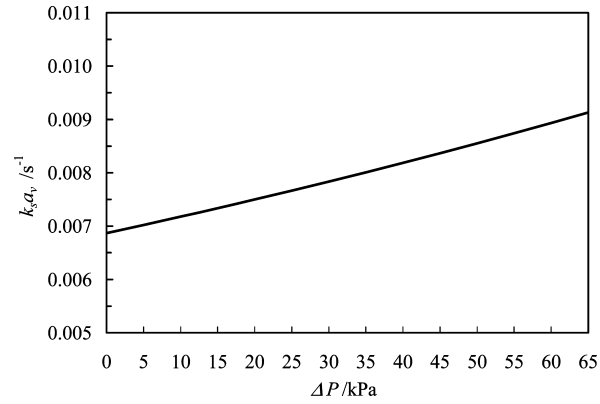

Figure 11. Effective mass transfer coefficient, k_sa_v vs pressure difference at an adsorption temperature of 30 °C.

Figures 5 and 6, respectively. Linear regressions can be yielded through the origin for most parts of the isotherms, which validate the appropriateness of the LDF model (eq 3). From eq 3, the adsorption rate constant or effective mass transfer coefficient, k_sa_v, can be calculated from the gradient of the regression line. The deviation between LDF predicted uptake (eq 4) and experimental uptake is satisfactorily found to be within 10 % as shown in Figure 7. Table 2 summarizes the k_sa_v under various pressure differences for adsorption temperatures of 30 °C and 35 °C. It can be seen that the k_sa_v obtained is between (0.0075 and 0.01013) L·s^{-1}. Plots of ln(k_sa_v) versus ΔP which are shown in Figure 8 are found to be linear with an R-square value above 0.95. From this, the correlations of the k_sa_v with pressure difference ΔP are obtained.

$$k_sa_v = 0.00687 \cdot \exp(0.00438 \cdot \Delta P), \quad T = 30\ ^\circ\mathrm{C} \tag{16}$$

Table 3. Comparisons of the Experimental k_sa_v, Predicted k_sa_v, and Arrhenius k_sa_v

T (°C)	ΔP (kPa)	k_sa_v(exp) (s^{-1})	k_sa_v(pre) (s^{-1})	k_sa_v(Arr) (s^{-1})	$\lvert(k_sa_v(\mathrm{exp}) - k_sa_v(\mathrm{pre}))/(k_sa_v(\mathrm{exp}))\rvert$ (%)	$\lvert(k_sa_v(\mathrm{exp}) - k_sa_v(\mathrm{Arr}))/(k_sa_v(\mathrm{exp}))\rvert$ (%)
30	21.0	0.00750	0.00753	0.00756	0.40	0.80
	32.0	0.00800	0.00790	0.00794	1.25	0.75
	43.0	0.00840	0.00829	0.00833	1.30	0.83
	62.0	0.00900	0.00901	0.00906	0.11	0.67
35	22.0	0.00830	0.00833	0.00831	0.36	0.12
	30.0	0.00868	0.00865	0.00866	0.35	0.23
	40.0	0.00915	0.00914	0.00912	0.11	0.33
	60.0	0.01010	0.01013	0.01011	0.30	0.10

$$k_s a_v = 0.00790 \cdot \exp(0.00514 \cdot \Delta P), \quad T = 35\ ^\circ\mathrm{C} \tag{17}$$

On the other hand, $\ln(D_{so}^*)$ versus various pressure differences can be calculated through eq 15 and the experimental $k_s a_v$. The results are plotted in Figure 9, from which the correlations of the D_{so}^* with pressure differences are obtained.

$$D_{so}^* = 0.00701 \cdot \exp(0.00438 \cdot \Delta P), \quad T = 30\ ^\circ\mathrm{C} \tag{18}$$

$$D_{so}^* = 0.00754 \cdot \exp(0.00514 \cdot \Delta P), \quad T = 35\ ^\circ\mathrm{C} \tag{19}$$

Therefore, the adsorption rate constant $k_s a_v$ in the Arrhenius form can be obtained (eq 15). A comparison of the experimental $k_s a_v$, predicted $k_s a_v$ (eqs 16 and 17), and Arrhenius $k_s a_v$ (eqs 15, 18, and 19) is presented in Table 3, which exhibits a good agreement with errors less than 2 %. Figure 10 presents the good approximation of the uptake predicted by the proposed equations and the uptake determined using the Arrhenius form to the experimental measured uptake (at pressure differences of 32 kPa under an adsorption temperature of 30 °C).

For general interpretation of the relation between $k_s a_v$ and pressure, the $k_s a_v$ versus pressure difference based on eq 16 is plotted as shown in Figure 11. If the gasoline vapor or the evaporator pressure is lower than the adsorber bed pressure, $k_s a_v$ will be less than 0.00687 at zero pressure difference. This correlation suggests that the pressure effect shall be taken into account in the adsorption kinetics for an adequate and accurate dynamic modeling and performance assessment.

Conclusions

The effect of initial bed pressure on the adsorption kinetics for gasoline on activated carbon of type Maxsorb III has been successfully measured by using a thermogravimetric analyzer (TGA) unit. Experiments have been conducted within the pressure differences between gasoline vapor and adsorption chamber from 20 kPa to 62 kPa under the adsorption temperatures of 30 °C and 35 °C. The linear driving force (LDF) model was satisfactorily used to express the adsorption kinetics. The effect of pressure on the effective mass transfer coefficient or adsorption rate constant can be explained by transition theory. The effective mass transfer coefficient exhibits an exponential change with the pressure difference under the isothermal adsorption process. The lower the initial chamber pressure or the higher the pressure difference, the higher are the adsorption rate and uptake. This study suggests that for the practical design of gasoline evaporative emission control or gasoline vapor recovery systems, a lower initial chamber pressure or higher vacuum chamber condition is preferred. However, the initial chamber pressure is constrained by the respective system design to suit for the actual working conditions.

Supporting Information Available:

The experimental adsorption uptake data for the adsorption temperatures of 30 °C and 35 °C under various pressure differences. This material is available free of charge via the Internet at http://pubs.acs.org.

Literature Cited

(1) Ntziachristos, L.; Mamakos, A.; Samaras, Z.; Xanthopoulos, A.; Iakovou, E. Emission Control Options for Power Two Wheelers in Europe. *Atmos. Environ.* **2006**, *40*, 4547–4561.

(2) Van der Westhuisen, H.; Taylor, A. B.; Bell, A. J.; Mbarawa, M. Evaluation of Evaporative Emissions from Gasoline Powered Motor Vehicles under South African Conditions. *Atmos. Environ.* **2004**, *38*, 2909–2916.

(3) Glueckauf, E. Theory of Chromatography, Part 10: Formula for Diffusion into Spheres and Their Application to Chromatography. *Trans. Faraday Soc.* **1955**, *51*, 1540.

(4) Li, Z.; Yang, R. T. Concentration Profile for Linear Driving Force Model for Diffusion in a Particle. *AIChE J.* **1999**, *Vol.45* (1), 196–200.

(5) Fletcher, A. J.; Yüzak, Y.; Thomas, K. M. Adsorption and Desorption Kinetics for Hydrophilic and Hydrophobic Vapors on Activated Carbon. *Carbon* **2006**, *44*, 989–1004.

(6) Malek, A.; Farooq, S. Kinetics of Hydrocarbon Adsorption on Activated Carbon and Silica Gel. *AIChE J.* **1997**, *43* (3), 761–776.

(7) Scholl, S.; Kajszika, H.; Mersmann, A. Adsorption and Desorption Kinetics in Activated Carbon. *Gas Sep. Purif.* **1993**, *7* (4), 207–212.

(8) El-Sharkawy, I. I.; Saha, B. B.; Koyama, S.; Ng, K. C. A Study on the Kinetics of Ethanol-Activated Carbon Fiber: Theory and Experiments. *Int. J. Heat Mass Transfer* **2006**, *49* (17−18), 3104–3110.

(9) Saha, B. B.; El-Sharkawy, I. I.; Chakraborty, A.; Koyama, S.; Yoon, S. H.; Ng, K. C. Adsorption Rate of Ethanol on Activated Carbon Fibre. *J. Chem. Eng. Data* **2006**, *51*, 1587–1592.

(10) El-Sharkawy, I. I.; He, J. M.; Ng, K C.; Yap, C.; Saha, B. B. Adsorption Equilibrium and Kinetics of Gasoline Vapors onto Carbon-Based Adsorbents. *J. Chem. Eng. Data* **2008**, *53* (1), 41–47.

(11) Ryu, Y. K.; Chang, J. W.; Jung, S. Y.; Lee, C. H. Adsorption Equibrilia of Toluene and Gasoline on the Activated Carbon. *J. Chem. Eng. Data* **2002**, *47*, 222–1225.

(12) Ryu, Y. K.; Chang, J. W.; Jung, S. Y.; Lee, C. H. Adsorption Equibrilia of Toluene and Gasoline on DAY Zeolite. *J. Chem. Eng. Data* **2002**, *47*, 363–366.

(13) Bansal, R. C.; Goyal, M. *Activated Carbon Adsorption*; Taylor & Francis, 2005.

(14) Otowa, T.; Tanibata, R.; Itoh, M. Production and Adsorption Characteristics of MAXSORB: High-Surface-Area Active Carbon. *Gas Sep. Purif.* **1993**, *7* (4), 241–245.

(15) Latham, L.; Burgeww, A. E. *Elementary Reaction Kinetics*; Butterworths: London, 1977.

(16) He, J. M. Adsorption Evaporative Emission Control System for Vehicle, Report of Mechanical Engineering Department, National University of Singapore, Report No. HT050329B, **2006**.

Received for review October 30, 2008. Accepted March 7, 2009.

JE800809K